Supporting Information

High-capacity hexaazatrinaphthylene anode for aqueous organic hybrid

flow battery

Zirui Liu [a]†, Zheng Wang [a]†, Yanjun Shi [a], Yong-Miao Shen [b], Wenchang Wang [a],

Zhidong Chen [a], Juan Xu *[a] and Jianyu Cao *[a]

[a]*Jiangsu Key Laboratory of Advanced Catalytic Materials and Technology, Changzhou*

University, Changzhou 213164, China.

[b]*Department of Chemistry, Zhejiang Sci-Tech University, Hangzhou 310018, China.*

†Z. L. and Z. W. contributed equally.

*Corresponding author. E-mail: jycao@cczu.edu.cn (Jianyu Cao);

cjytion@cczu.edu.cn (Juan Xu)

Electron transfer coefficient (α) and charge transfer rate constant (k⁰) for ET1 and

ET2

   Fig. S1 shows CVs of HATN electrode in 1 M KOH solution at different scan

rates (v). The scan rates increase from 0.2 to 4 V s⁻¹. The α and k^0 were determined by

Laviron's method [S1] from the following equation:

$$\Delta E_p = \frac{2.303RT}{\alpha(1-\alpha)nF}\left[\alpha\log(1-\alpha) + (1-\alpha)log\alpha - \log\left(\frac{RTk^0}{nF}\right)\right] + \frac{2.303RT}{\alpha(1-\alpha)nF}logv \quad \textbf{(Eq. S1)}$$

where ΔE_p is the potential difference between the oxidation and reduction peak, v is the

scan rate, n is the transfer electron number ($n=3$), k^0 is charge transfer rate constant, and α is electron transfer coefficient, respectively.

The plot of ΔE_p versus log(v) produces a straight line along with an intercept at high scan rates (**Fig. S2a and S2b**). The k^0 is obtained from the intercept value. The α value for both ET1 and ET2 of HATN can be calculated from the slope of the ΔE_p-log (v) dependence ($2.3RT/\alpha(1-\alpha)nF$), which is about 0.74 and 0.53, respectively. Then, the k^0 value for ET1 and ET2 is calculated to be ca. 9.66 and 33.3 s^{-1}, respectively.
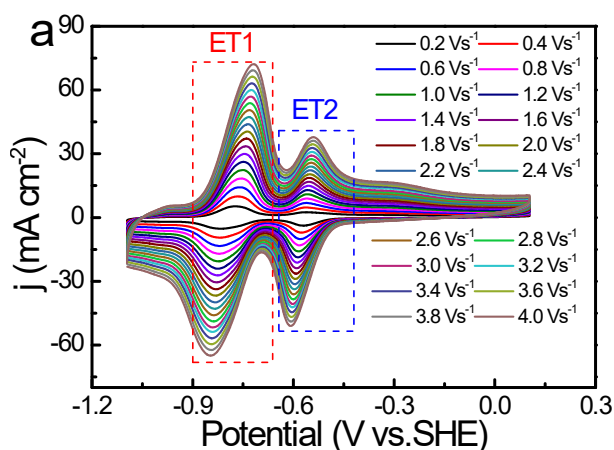

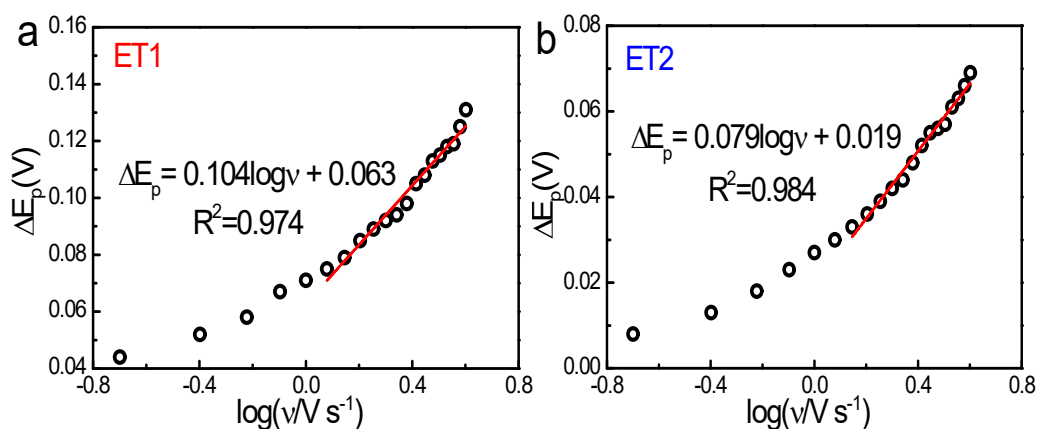**Fig. S1** CVs of HATN electrode in 1 M KOH solution at different scan rates (the scan rates (v) from 0.2 to 4 V s^{-1}).

Fig. S2 (a) Plot of ΔE_p versus log (v) for ET1 of HATN electrode. (b) Plot of ΔE_p versus log (v) for ET2 of HATN electrode.
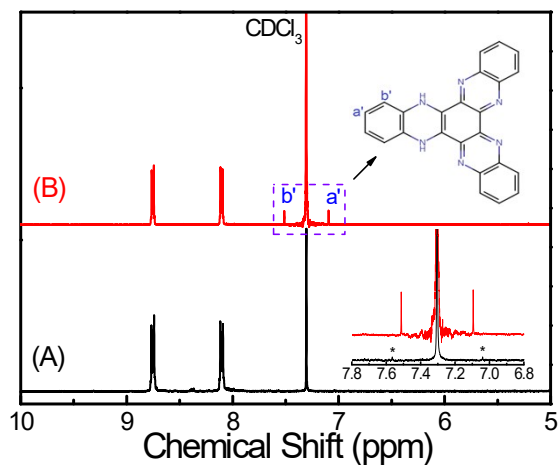
Fig. S3 ^{1}H NMR (500 MHz, CDCl$_3$) spectra. (A) as-synthesized HATN. (B) HATN after 7 days treating in 1 M KOH at 25 °C.

The as-synthesized HATN (11.5 mg) was added to 20 mL of 1 M KOH solution with intense magnetic stirring at room temperature and kept for 7 days. Then, 20 mL of chloroform was added to dissolve HATN and extract possible decomposition products. After the chloroform was removed by rotary evaporation, about 0.5 mL deuterated chloroform was added to form a saturated solution of HATN that was used as the sample for the ^{1}H NMR analysis. Two additional proton peaks located at 7.51 and 7.09 ppm were observed in the ^{1}H NMR spectrum of the HATN sample after 7 days treating in 1 M KOH, which was assigned to hydrogenated hexaazatrinaphtylene (*e.g.* HATN-2H, a by-product of HATN) that was enriched during sample processing.

Table S1. Summary of various hybrid RFBs. j, current density; AC, areal capacity; μ, mass loading of anode material; η, material utilization. NA, not applicable.

Flow cell	j (mA cm^{-2}) [a]	AC (mAh cm^{-2}) [b]	μ (mg cm^{-2}) [c]	η [d]	Cycle number	Anolyte
Zn-polyiodide [S2]	10	234.3	429.2	66.6%	38	3.5 M ZnI$_2$
Zn-Br$_2$&I$_2$ [S3]	10	34	122.6	33.8%	20	5M ZnI$_2$ + 2.5 M ZnBr$_2$
Zn-Br$_2$ single [S4]	80	23.2	58[e]	48.7%[e]	500	3M ZnBr$_2$
Zn-Br$_2$ [S5]	40	40	726.7	6.7%	140	2 M ZnBr$_2$
Zn-Br$_2$ [S6]	100	20	545	4.5%	5000	2 M ZnBr$_2$ + 0.5 M ZnCl$_2$
Zn-Fe [S7]	100	26.3	40.9	78.5%	210	0.5 M Zn(OH)$_4^{2-}$
Zn-Mn [S8]	40	13.3	54.5	30.0%	100	1.5 M ZnCl$_2$
Zn-poly(TEMPO) static [S9]	2	0.108	3.14	4.2%	1000	0.08 M ZnCl$_2$
Zn-TEMPO-SO$_3$K [S10]	40	~20	261.6	9.3%	50	2 M ZnCl$_2$
PPyQX-K$_4$Fe(CN)$_6$ [S11]	~1.5 (4 A g^{-1})	0.18	0.37	24.2% (at 1 Ag^{-1})	1000	NA
TPPHZ-K$_4$Fe(CN)$_6$ [S12]	10.2 (10 A g^{-1})	0.09	1.02	71.7% (at 1 Ag^{-1})	1200	NA
HATN-K$_4$Fe(CN)$_6$ (this work)	20 (8 A g^{-1})	0.668	2.5	63.9% (at 0.5 Ag^{-1})	1500	NA

[a]The applied current density during the long-term charge-discharge cycling. [b]Areal capacity is obtained by dividing the achieved reversible capacity by the active electrode area. [c]The mass loading of anode material (μ) is calculated using the following formula:

$$\mu = \frac{nCVF}{3.6A}$$

(Eq. S1)

where n is the number of electrons per mole, C is the concentration of zinc ion in the

anolyte, V is volume of the anolyte, F is the Faraday constant and A is the electrode

area. [d]The material utilization (η) is obtained by dividing the achieved reversible

capacity by the theoretical capacity of the anolyte or the solid anode material. [e]Based
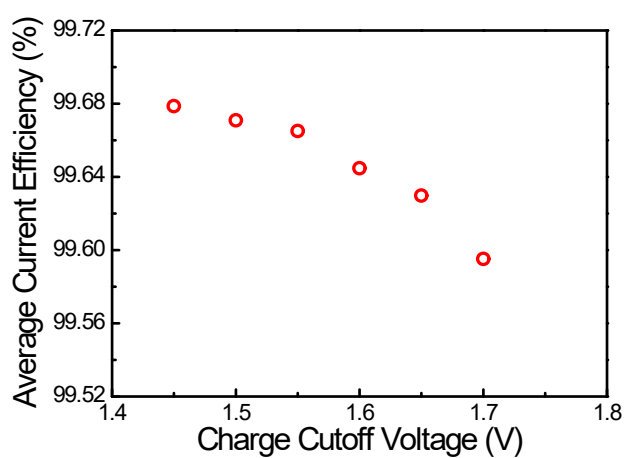
on the volume of anolyte of 14.2 mL.

Fig. S4 Average current efficiency of the HATN//K$_4$[Fe(CN)$_6$] cell versus charge cut-

off voltage at a constant current density of 8 A g^{-1}.

Table S2 Performance comparisons of the HATN//K$_4$[Fe(CN)$_6$] AHFB with other previously-reported organic AHFBs. OCV, open circuit voltage (in V); SDC, specific discharge capacity; CE, Coulomb efficiency; EE, energy efficiency; CRPC, capacity retention per cycle. NA, not applicable. All performances data are obtained at room temperature.

AHFB	OCV	SDC	CE	EE	CRPC
Zn//poly(TEMPO) [S9]	1.70 V	1.1 AhL^{-1a}	~98% (at 0.01A cm^{-2})	81% (at 0.01A cm^{-2})	~99.977% (1000 cycles)
Zn//TEMPO-SO$_3$K [S10]	1.69 V	0.92 AhL^{-1a}	>98% (at 0.003 A cm^{-2})	>86% (at 0.003 A cm^{-2})	99.994% (1100 cycles)
Zn//FQ [S13]	~2.0 V	~4.5 AhL^{-1a}	99.5% (at 0.02A cm^{-2})	70.2% (at 0.02A cm^{-2})	99.92% (50 cycles)
Zn//pBQ [S14]	>1.17 V	NA	~72% (at 0.03A cm^{-2})	42% (at 0.03A cm^{-2})	NA (20 cycles)
Zn//g$^+$-TEMPO [S15]	~1.6 V	~4.2 AhL^{-1a}	99.3% (at 0.02 A cm^{-2})	77.1% (at 0.02 A cm^{-2})	99.954% (140 cycles)
PAQP$_y$//NH$_2$-TEMPO [S16]	1.02 V	23.9 mAhg^{-1}(at 0.2 Ag^{-1})^b	NA	53.9% (at 1A g^{-1})	99.80% (100 cycles)
PAQP$_y$/G//NH$_2$-TEMPO [S16]	1.02 V	62.2 mAhg^{-1}(at 0.2 Ag^{-1})^b	92% (at 1A g^{-1})	74.5% (at 1A g^{-1})	99.68% (100 cycles)
PPyQX//K$_4$[Fe(CN)$_6$] [S11]	1.15 V	67.1 mAhg^{-1}(at 1 Ag^{-1})^b	93.8% (at 4 A g^{-1})	80.5% (at 4 A g^{-1})	~99.975% (1000 cycles)
TPPHZ//K$_4$[Fe(CN)$_6$] [S12]	1.37 V	92.4 mAhg^{-1}(at 1 Ag^{-1})^b	98.6% (at 10 A g^{-1} or 10.2 mA cm^{-2})	87.2% (at 10 A g^{-1} or 10.2 mA cm^{-2})	99.998% (1200 cycles)
TPPHZ/G//K$_4$[Fe(CN)$_6$] [S17]	1.30 V	87.1 mAhg^{-1}(at 0.5 Ag^{-1})^b	95.1% (at 5 A g^{-1} or 5.5 mA cm^{-2})	89.3% (at 5 A g^{-1} or 5.5 mA cm^{-2})	~99.9938% (3000 cycles)
HATN//K$_4$[Fe(CN)$_6$] in this work	~1.14 V	267 mAhg^{-1}(at 0.5 Ag^{-1})^b	99.7% (at 8 A g^{-1} or 20 mA cm^{-2})	75.5% (at 8 A g^{-1} or 20 mA cm^{-2})	~99.977% (1500 cycles)

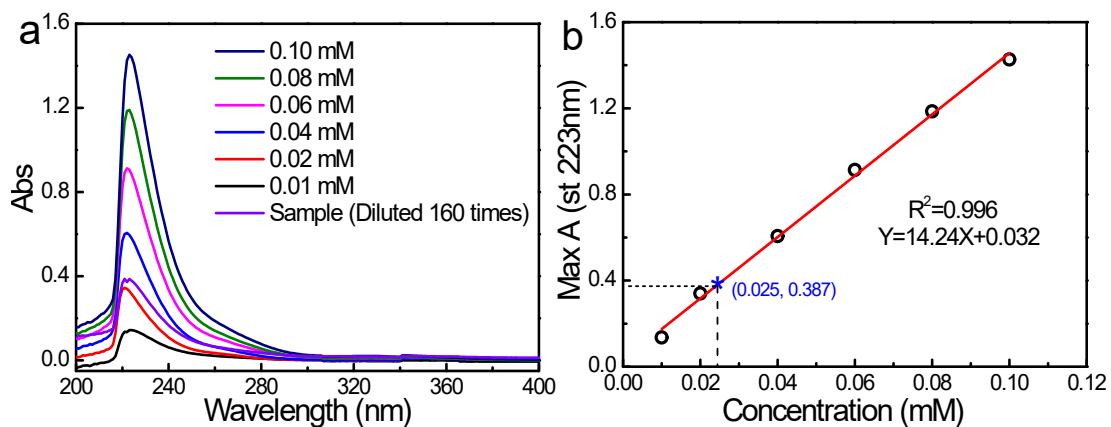^{a}Based on the catholyte. ^{b}Based on the anode material.

Fig. S5 (a) UV-vis absorption spectra of the $K_4Fe(CN)_6$ solution with different concentration. (b) The linear plot between the concentration of $K_4Fe(CN)_6$ and the maximum absorbance recorded at $\lambda=223$ nm. The concentration of $K_4Fe(CN)_6$ at the anode side (acceptor half cell) was calculated to be ~3.99 mM.
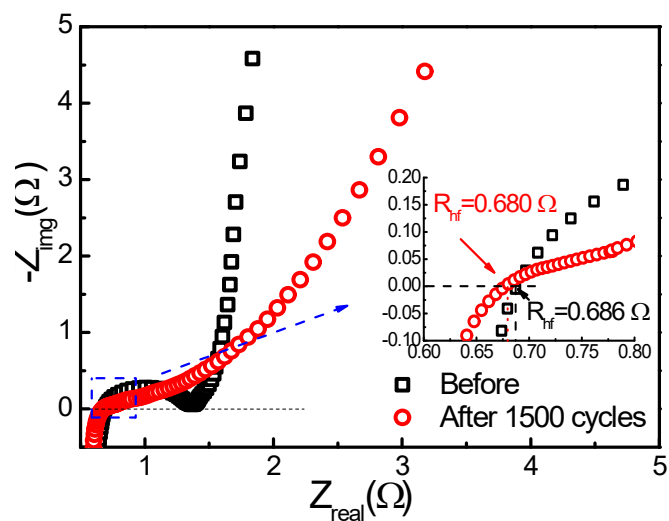

Fig. S6 EIS spectra of the HATN//$K_4Fe(CN)_6$ cell before and after 1500 cycles.
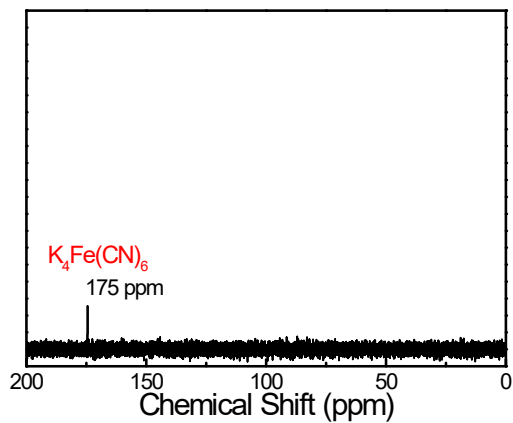
Fig. S7 ^{13}C NMR spectrum (125 MHz, D_2O) for the supporting electrolyte on the HATN side after 1440 cycles at 8 A g^{-1}.
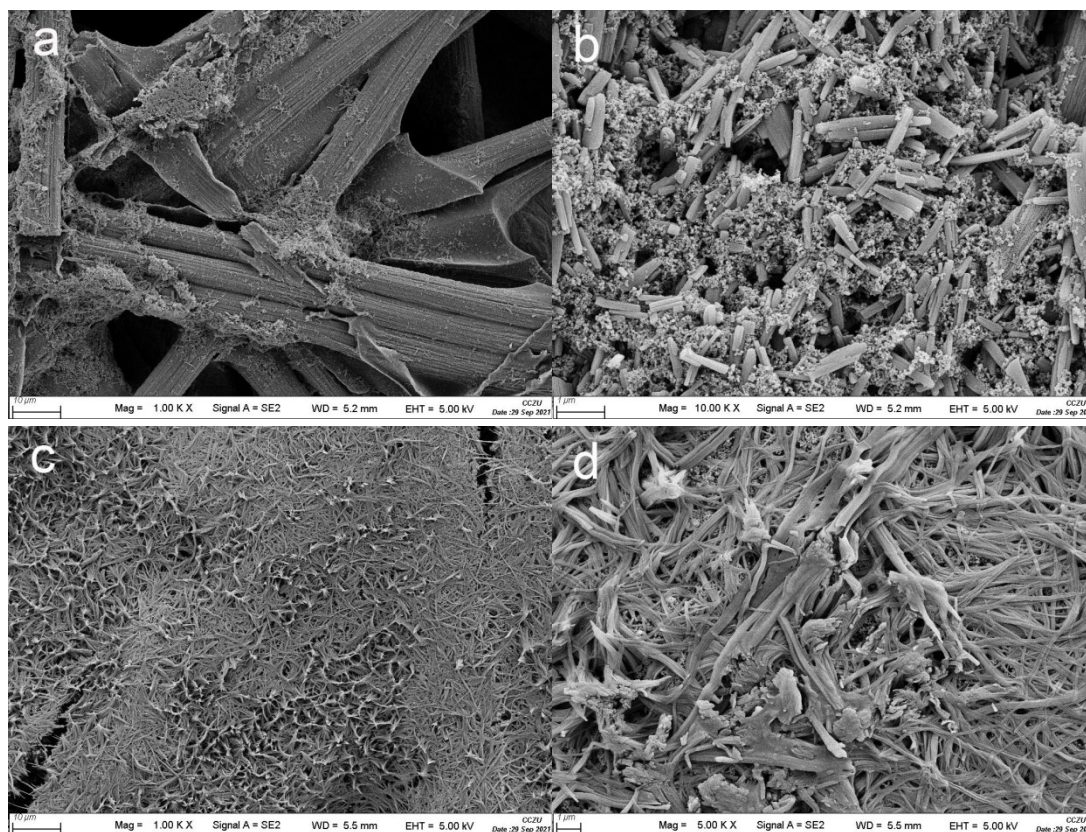

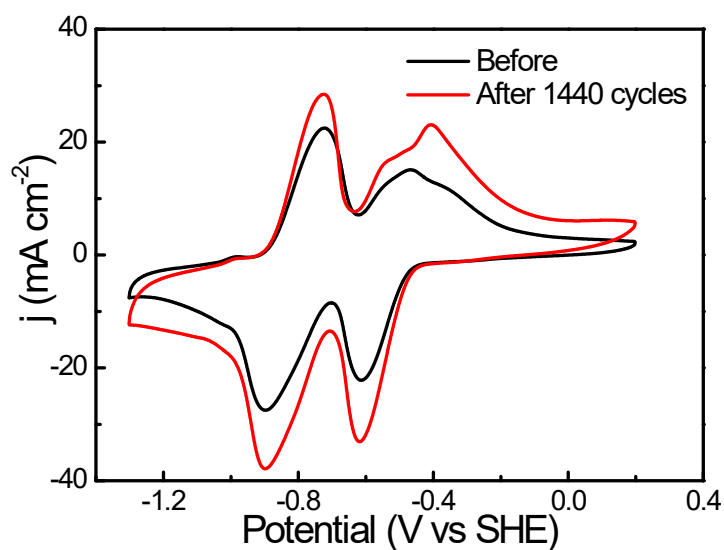**Fig. S8** SEM images of a HATN electrode. (a, b) before cycling. (c, d) after cycling.

Fig. S9 CV curves of the HATN electrode before and after 1440 cycles at 25 mVs^{-1}.
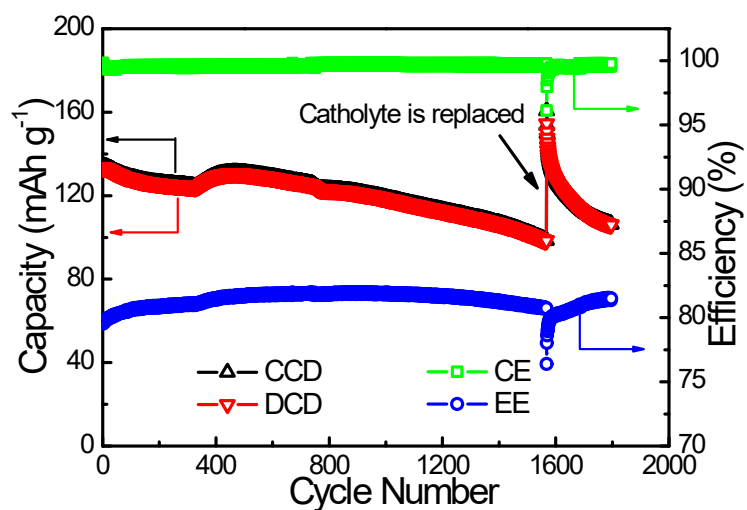

Fig. S10 Cycling capacity retention and efficiency data of the HATN//K$_4$[Fe(CN)$_6$] cell at 8 A g^{-1}. 1 M KOH + 0.35 M KCl solution (10 mL) was used as the anodic supporting electrolyte while 50 mM K$_4$[Fe(CN)$_6$] + 50 mM K$_3$[Fe(CN)$_6$] in 1 M KOH solution (10 mL) was used as the catholyte. After 1568 cycles, the Fe(CN)$_6^{4-}$/Fe(CN)$_6^{3-}$ catholyte was replaced with a fresh one.

References

[S1] (a) Laviron, E. *J. Electroanal. Chem.* 1979, 101, 19; (b) S. Chatterjee, K. Sengupta, S. Bandyopadhyay, A. Dey, *J. Mater. Chem. A* 2016, 4, 6819.

[S2] B, Li, Z. Nie, M. Vijayakumar, G. Li, J. Liu, V. Sprenkle, W. Wang, *Nat. Commun.* 2015, 6, 6303.

[S3] G.-M. Weng, Z. Li, G. Cong, Y. Zhou, Y.-C. Lu, *Energy Environ. Sci.* 2017, 10, 735.

[S4] C. Xie, Y. Liu, W. Lu, H. Zhang, X. Li, *Energy Environ. Sci.* 2019, 12, 1834.

[S5] Y. Yin, S. Wang, Q. Zhang, Y. Song, N. Chang, Y. Pan, H. Zhang, X. Li, *Adv. Mater.* 2020, 32, 1906803.

[S6] J.-H. Lee, R. Kim, S. Kim, J. Heo, H. Kwon, J. H. Yang, H.-T. Kim, *Energy Environ. Sci.* 2020, 13, 2839.

[S7] Z. Yuan, Y. Duan, T. Liu, H. Zhang, X. Li, *iScience* 2018, 3, 40.

[S8] C. Xie, T. Li, C. Deng, Y. Song, H. Zhang, X. Li, *Energy Environ. Sci.* 2020, 13, 135.

[S9] J. Winsberg, T. Janoschka, S. Morgenstern, T. Hagemann, S. Muench, G. Hauffman, J.-F. Gohy, M. D. Hager, U. S. Schubert, *Adv. Mater.*, 2016, 28, 2238.

[S10] J. Winsberg, C. Stolze, A. Schwenke, S. Muench, M. D. Hager, U. S. Schubert, *ACS Energy Lett.*, 2017, 2, 411.

[S11] B. Wang, Y. Zhang, Y. Zhu, Y.-M. Shen, W. Wang, Z. Chen, J. Cao, J. Xu, *J.*

Power Sources 2020, 451, 227788.

[S12] Y. Zhang, J. Cao, Z. Chen, J. Xu, C. Yu, *J. Mater. Chem. A* 2020, 8, 6874.

[S13] M. Park, E. S. Beh, E. M. Fell, Y. Jing, E. F. Kerr, D. DePorcellinis, M.-A. Goulet, J. Ryu, A. A. Wong, R. G. Gordon, J. Cho and M. J. Aziz, *Adv. Energy Mater.*, 2019, 1900694.

[S14] P. K. Leung, T. Martin, A. A. Shah, M. R. Mohamed, M. A. Anderson and J. Palma, *J. Power Sources*, 2017, 341, 36.

[S15] Z. Chang, D. Henkensmeier, R. Chen, *ChemSusChem*, 2017, 10, 3193-3197.

[S16] J. Cao, F. Ding, H. Chen, H. Wang, W. Wang, Z. Chen, J. Xu, *J. Power Sources* 2019, 423, 316-322.

[S17] Y. Zhang, W. Liu, Z. Wang, Y.-M. Shen, W. Wang, Z. Chen, J. Xu, J. Cao, *Carbon* 2020, 161, 309-315.